A Wave Optics Propagation Code for Multi-Conjugate Adaptive Optics

B. L. Ellerbroek
Gemini Observatory, 670 N. A'ohoku Place, Hilo HI 96720 USA

Gemini Preprint #69

A Wave Optics Propagation Code for Multi-Conjugate Adaptive Optics

Venice 2001
Beyond Conventional Adaptive Optics

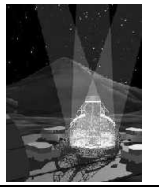

B.L. Ellerbroek

Gemini Observatory, 670 N. A'ohoku, Hilo, HI 96720, USA

ABSTRACT

We describe the purpose and sample results of a wave optics propagation simulation developed to study multi-conjugate adaptive optics for 4-10 m class telescopes. This code was developed to assess the impact of diffraction effects and a variety of implementation error sources upon the performance of the Gemini-South MCAO system. These effects include: Hartmann sensing with extended and elongated laser guide stars, optical propagation effects through the optics and atmosphere, laser guide star projection through the atmosphere, deformable mirror and wave front sensor misregistration, and calibration for non-common path errors. The code may be run in either a wave optics or geometric propagation mode to allow the code to be anchored against linear analytical models and to explicitly evaluate the impact of diffraction effects. The code is written in MATLAB, and complete simulations of the Gemini-South MCAO design (including 3 deformable mirrors with 769 actuators, 5 LGS WFS with 1020 subapertures, 3 tip/tilt NGS WFS, and 50 meter phase screens with 1/32nd meter resolution) are possible using a Pentium III but require 1 to 6 days. Sample results are presented for the Gemini-South MCAO system.

1. INTRODUCTION

The subject of performance evaluation for multi-conjugate adaptive optics (MCAO) (Beckers 1989) has already received considerable attention. Numerous studies of predicted performance are now available, many of them using analytical methods (Ellerbroek 1994 and 2000, Fusco et. al 2000, Johnston and Welsh 1994) that are generalizations of techniques previously used to evaluate simpler adaptive optics (AO) systems (Tyler 1994, Walner 1983, Welsh and Gardner 1991). Monte Carlo simulations have also been used to estimate MCAO performance (Flicker et. al 2000). All of these methods have obtained broadly consistant results. This is not too surprising, since they are all based upon a common first-order model for the AO system and the turbulence-induced phase errors to be corrected. Some of the basic elements of this model include: Optical phase distortions obtained by geometric ray tracing through the atmophere and optical system, wave front sensor measurements that are linear functions of these phase profiles summed with additive noise, and a perfectly aligned and calibrated AO system.

These assumptions simplify the computation of optimal reconstruction algorithms and best-case performance estimates for an ideal MCAO system, but higher-fidelity models will be required to address a range of more involved issues as the design work on real MCAO systems progresses. Some of these issues include: (i) The nonlinearities and dynamic range limitations of Shack Hartmann (SH) sensors and other wave front sensing approaches; (ii) scintillation and diffration effects in the optics and atmosphere; (iii) laser guide star (LGS) elongation, aberrations, and pointing errors; (iv) deformable mirror (DM) and wave front sensor (WFS) misregistration errors; (v) non-common path wave front errors; (vi) WFS gain and bias calibration in the presence of the above; and (vii) AO control loop temporal dynamics. We are now developing a Monte Carlo wave optics propagation simulation to investigate these higher-order effects. This paper provides an overview of some of the results generated so far for the planned Gemini-South MCAO system.

Recent advances in microprocessor performance have greatly reduced the drudgery involved in developing and applying a propagation simulation to model a very-high-order AO system on a large telescope. Some of the improvement in processor speed can be given back to allow the use of higher-level languages, such as MATLAB or IDL, that provide a much more efficient and flexible development environment at the expense of some reduction in efficiency. Very large simulation cases are still tractable using this approach. The Gemini-South MCAO

Layer	Altitude, m	Fractional Strength	Windspeed, m/s
1	0	0.6475	5.0
2	2077	0.1111	10.0
3	3414	0.0774	15.0
4	5562	0.0439	20.0
5	7212	0.0245	30.0
6	13091	0.0810	20.0
7	15840	0.0146	10.0

Table 1. Atmospheric Turbulence and Windspeed Profiles

This profile is based upon median seeing condtions at Cerro Pachon. Note that the layer altitudes are expressed in terms of the altitude above the site.

simulation, for example, includes 3 DM's with a total of 769 actuators, 3 natural guide star (NGS) and 5 LGS WFS's with a total of 1026 subapertures, and 7 atmospheric phase screens with an extent of 52.5 meters and a spatial resolution of 3.125 or 6.25 centimeters. These cases can be run on a 1 GHz Pentium III with 768 Mbytes of RAM, although the ratio between computer time and simulated time is in the range from 10^5 to 5×10^6, depending upon the range of simulation features included from the above list. This is still efficient enough to enable simulation runs to be completed in from a few hours to less than a week. These simulation results can be used to help quantify the impact of many MCAO system design parameters (e.g. the allowable DM-to-WFS misregistration) and increase confidence in MCAO performance predictions before the system is actually built. The significant costs and predicted high payoffs associated with implementing MCAO on 8 to 10 meter class telescopes make detailed and accurate modeling particularly important. This will be even more true for extremely large telescopes (ELT's), where wave optics propagation simulations of MCAO should still be possible using parallel processing.

In the remainder of this paper, we present a range of sample simulation results generated in support of the Prelimenary Design Review for the Gemini-South MCAO system. The principal goals of these studies were to validate previous analytical performance estimates, and to understand how MCAO performance is influenced by higher-order effects such as diffraction, DM misregistration, and three-dimensional laser guide stars. Section 2 outlines the parameters used in these simulations. Section 3 compares ideal simulation results, obtained without including diffraction, WFS noise, or misregistration effects, against analytical MCAO performance predictions. The results in Section 4 illustrate the impact of diffraction effects in the WFS, MCAO optical system, and the atmosphere. Finally, Section 5 describes simulations that include WFS measurement noise and DM-to-WFS misregistration.

2. PARAMETER SUMMARY

The simulation results described in this paper are based upon a 7-layer discrete fit to the median Cerro Pachon atmospheric turbulence profile. The altitudes, relative strengths, and windspeeds for the 7 layers are listed in Table 1. The simulated seeing corresponds to $r_0 = 0.166\,\mathrm{m}$ at a wavelength of 0.5 microns, and the isoplanatic angle is approximately 2.75 arc seconds. Table 2 lists the basic AO system parameters used for the all of the simulations unless indicated otherwise. These values are generally in close agreement with the parameters for the Gemini-South MCAO design except as noted in the table caption.

One feature of the wavefront reconstruction algorithm used in these simulations that deserves discussion is the treatment of partially illuminated WFS subapertures at the edge of the pupil, as well as edge DM actuators that couple very weakly into the WFS measurements. For simulations using the geometric optics WFS model, the DM-to-WFS influence matrix G is still known accurately for all edge subapertures and actuators, and all of these elements can be used for wave front control using the standard formula for the minimal variance wave front reconstructor. In simulations (and real world AO system) using wave optics, we have found that it can be very difficult to properly calibrate the WFS measurements from weakly illuminated subapertures on account of (i) the different shape of the Shack-Hartmann spot, and (ii) the differences in the influence matrix coefficients. AO loop performance consequently appears to be more sensitive to misregistration and non-common path wave front errors when measurements from very weakly illluminated WFS subapertures are used for wave front reconstruction. In these simulations, the WFS measurement vector is restricted to measurements from

Laser Subsystem Parameters		
Number of LGS	5	
LGS locations in field	$(0'', 0'')$ and $(\pm 30'', \pm 30'')$	
LGS signal level at WFS	125 PDE's s/cm^2/sec	
Transmitted beam quality	Diffraction limited	
Beam $1/e^2$ diameter	0.3 m	
Launch telescope diameter and location	0.45 m, on-axis	
Sodium layer range	99 km	
Adaptive Optics Module		
Number of DM's	3	
Conjugate ranges	0.0, 4.5, 9.0 km	
Actuator pitch	$D/16$, $D/16$, $D/8$	
Number of WFS	5 (LGS)	4 (NGS)
WFS order	16 by 16	Tip/tilt
WFS pixel subtense on the sky	1.0 arc sec	0.5 arc sec
WFS read noise	6 electrons	0 electrons
WFS sampling rate	800 Hz	
Control System		
Control algorithm	Minimal variance	
Processing latency + read time	1.25 ms	
-3 dB closed loop bandwidth	32 Hz	

Table 2. MCAO System Simulation Parameters

These parameters were used for all of the simulations described in this paper except where otherwise indicated. D is the telescope aperture diameter (8 meters), and PDE is an abbreviation for photodetection events. These parameters correspond to the Gemini-South MCAO system design with the following exceptions: A diffraction-limited laser beam (vs 1.5 xDL), an integrated wavefront reconstruction algorithm for both LGS and NGS WFS measurements, and 4 instead of 3 NGS tip/tilt guide stars. This last modification yields symmetric performance over the 1 arc minute square field of view and simplifies performance evaluation.

subapertures that are at least 40% illluminated. This increases the number of DM edge actuators that couple into the pupil but are in the null space of G, and we have used a simple nearest-neighbor slaving algorithm for these actuators.

Of course, deleting edge subapertures and actuators in this fashion decreases the order of the AO system and may increase the residual wavefront fitting error, but analytical Strehl ratio calculations using these boundary conditions (based upon geometric optics) yield virtually no change in MCAO performance.

Finally, all simulations used a propagation grid mesh of 1/32 meter, a grid size of 1680 points, and a total grid width of 52.5 meters unless specified otherwise. Each simulation ran for 100 cycles, with mean Strehl ratios averaged over cycles 21-100.

3. PERFORMANCE ESTIMATES FOR GEOMETRIC OPTICS

We began this study with simulations using a geometric optics model in order to validate the simulation code against analytic performance predictions that should be exactly correct for this case. Strehl ratios were evaluated in J, H, and K bands (1.25, 1.65, and 2.2 microns), at the center, edge, and corner of a one square arc minute field of view. The edge and corner values were averaged over all four edges and corners. Table 3 summarizes the results obtained. The simulation Strehl ratios are slightly higher than the analytical calculations but consistantly agree to within 1-3 per cent. We believe that this discrepancy is primarily due to the finite outer scale introduced in the simulation by the use of periodic phase screens, which reduces the level of atmospheric turbulence present in the lower-order modes.

4. DIFFRACTION EFFECTS

Like Gaul, the effects of diffraction on MCAO simulation results may be divided into three parts: (i) Diffraction in the Shack-Hartmann wave front sensors; (ii) wave optics propagation effects in the atmosphere and optics;

Spectral Band	Analysis Strehls			Simulation Strehls		
	Center	Edge	Corner	Center	Edge	Corner
J	0.590	0.478	0.475	0.615	0.509	0.505
H	0.739	0.653	0.649	0.756	0.679	0.674
K	0.843	0.787	0.783	0.854	0.804	0.800

Table 3. MCAO Analysis vs Simulation Strehl Ratios with Geometric Optics

This table plots mean Strehl ratios at the center, edge, and corner of a square 1 arc minute field of view for the atmospheric and AO system parameters summarized in Tables 1 and 2 above.

and (iii) wave front sensing with extended laser guide stars. The following three subsections describe simulation results quantifying these effects for the Gemini-South MCAO design.

4.1. WFS Gain and Speckle Noise

The tilt measurement gain of a Shack-Hartmann wave front sensor can be viewed as the reciprocal of the width of the guide star image in each subaperture. The width and profile of this image can be estimated using an MTF approach that represents the time-averaged effect of uncompensated atmospheric turbulence as a transfer function, but this formula is only an approximation and the actual gain will be somewhat different. This is especially true for the NGS full aperture tip/tilt measurements, since these star images will be partially sharpened via the response of the closed loop AO system. WFS measurements computed from Shack-Hartmann spots will also differ from the ideal geometric measurements (i.e., the average wave front gradient on each subaperture) due to so-called "speckle noise," which is the error introduced in the quad cell tilt estimate by the residual aberrations in the shape and symmetry of the guide star images. Both of these effects must be understood to obtain satisfactory simulation results.

An AO simulation provides the opportunity to compute both types of WFS measurements simultaneously with the AO loop closed on the geometric measurements, so that the gain and randomness in the wave optics measurements can be easily quantified via a least squares fit. For the MCAO scenario considered here, the WFS gain estimates computed using the MTF approach are too small by factors of 1.15 and 1.8, respectively, for the LGS and NGS wave front sensors. These results were computed with diffraction effects modelled in the WFS's alone, with ideal point source laser guide stars and geometrical propagation through the atmosphere. The value of d/r_0 is about 2.5 for the LGS WFS measurements, so it is not surprising that the long-exposure MTF formula underestimates the WFS gain by a moderate amount. The result for the NGS WFS represents the amount that the PSF has been sharpened by the closed-loop AO system. The improvement is nontrivial but not particularly dramatic, and indicates the limited degree of compensation provided by the AO system at the NGS WFS wavelength of 0.7 microns.

Figure 1 plots the relationship between the closed loop NGS tip/tilt measurements computed using the diffraction and geometric WFS models. The best fit scale factor between the two sets of measurements is unity because the measurements computing by the diffraction model have already been scaled by 1.8^{-1}. Note that the residual NGS WFS measurements errors are very small: The RMS scatter in the fit is only 2.3 milli arc seconds. This is about 0.4 per cent of λ/r_0, indicating that the large number of speckles in the (very) partially compensated NGS image largely average out. This is a fortunate result, and it would be difficult to obtain with high confidence using any method except for simulation.

The corresponding level of speckle noise for the LGS WFS measurements is about 16.2 milli arc seconds. This is about 2.7 per cent of λ/r_0 at the sensing wavelength, which agrees with the intuition that the size of this error will be larger for a few speckles than for many speckles. This small value is still large enough to be a significant source of error for a wave front reconstruction if the control algorithm has been optimized for absolutely zero measurement noise. Figure 2 illustrates Strehl ratio time histories for the first few cycles of a MCAO simulation as a function of the mix of WFS models used, assuming infinite WFS signal levels and a reconstruction matrix optimized for this case. These are H band Strehl ratios at one particular point on the edge of the 1 square arc minute field. The results obtained using geometric models for both the LGS and NGS sensors approach values that are consistent with analytical predictions. Introducing diffraction effects in the NGS WFS has a relatively modest impact on the Strehl ratios achieved, although the Strehls do not begin to increase significantly until the higher-order AO system has started to sharpen the star images in the NGS

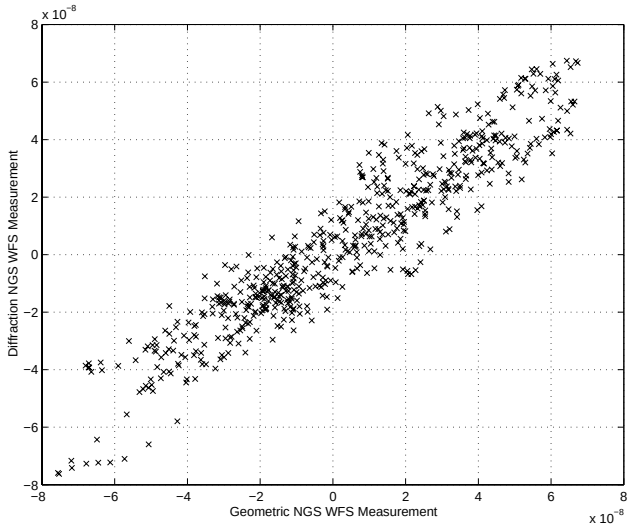

Figure 1. Wave Optics Effects on NGS WFS Measurements

This figure plots NGS tip/tilt measurements computed using a diffraction model for the Shack-Hartmann WFS against the measurements computed for a geometric WFS model (i.e., the average wavefront gradient on the aperture). Both sets of measurements were computed for the same residual wavefront errors with the AO loop closed, and the units are radians of full aperture tilt. The diffraction-based measurements have already been scaled to yield the best linear relationship, and the RMS of the residual scatter is about 0.011 microradians, or 2.3 milli arc seconds.

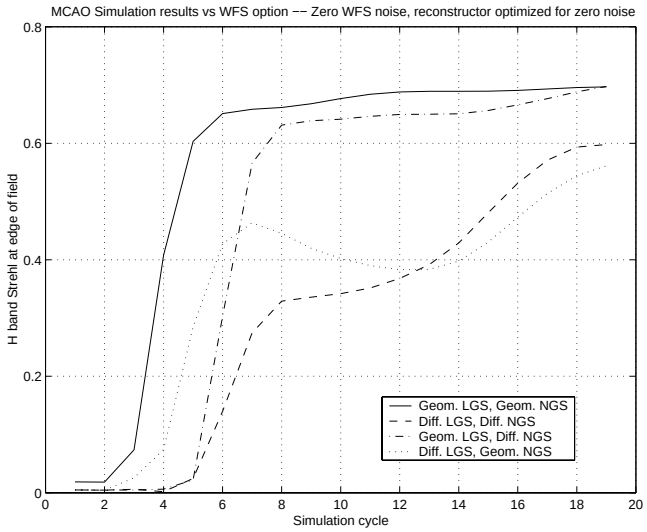

Figure 2. Impact of WFS Diffraction on MCAO Performance for a Reconstuctor Tuned for Zero Measurement Noise

This figure plots H band Strehl ratios at one point on the edge of the 1 arc second square field of view for the first few cycles of a MCAO simulation. The reconstruction algorithm has been optimized for noise-free WFS measurements, and is easily confused by the noise-like effects of diffraction in the LGS WFS.

WFS. The Strehl ratio "tax" for diffraction effects in the LGS WFS is much larger, and remains signficant for the entire simulation run. The loss in Strehl is larger than one might expect for WFS measurement noise of only 2.7 per cent of a blur diameter, but the effect is increased because (i) the error is highly correlated from one WFS measurement to the next, and (ii) speaking anthropomorphically, reconstruction algorithms are in a certain sense gullible if they have been designed to expect no WFS measurement noise at all.

Fortunately, this error source can be largely eliminated by using a more realistic (or cynical) reconstruction

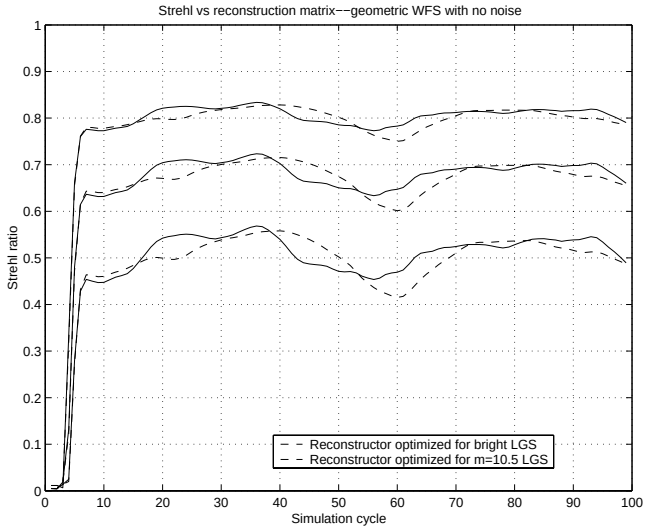

Figure 3. Simulation Results vs. Reconstruction Algorithm for a Geometric WFS Model with Zero Measurement Noise

This figure plots Strehl ratio time histories in J, H, and K bands for one point at the edge of 1 square arc minute MCAO field of view. The two reconstruction algorithms have been optimized for infinite WFS signal levels and zero measurement noise, and for the m=10.5 LGS actually specified for Gemini-South MCAO. The WFS measurements are actually noise-free and were computed using the geometric WFS model. The loss of performance for the suboptimal reconstructor corresponds to an RMS OPD of about 30 nanometers.

matrix that has been optimized for a small but non-zero level of WFS measurement noise. The resulting Strehl ratio penalty for using a suboptimal reconstructor corresponds to an RMS optical path difference (OPD) of about 30 nanometers (see Fig. 3), and the additional error induced by speckle noise in the LGS and NGS WFS's is a much more acceptable 50 nanometers (see the solid vs dashed curve in Fig. 4). This level of error due to diffraction effects is relatively tolerable, but it does not yet include the effects of wave optics propagation or extended laser guide stars.

4.2. Wave Optics Propagation Effects

The simulation results presented in the preceeding section are still for the case of of ideal point source laser guide stars and geometrical propagation (i.e., ray tracing) throught the optics and atmosphere. The dash-dot curve in Fig. 4 illustrates the effect when the nearfield Fresnel propagator is substituted for the geometrical model. The loss in the time-averaged Strehl ratios is very small, corresponding to an RMS OPD of no more than about 22 nanometers in the worst case. The impact of atmospheric scintillation and the suboptimal ordering of the DM's in the Gemini South MCAO design can therefore be neglected at IR wavelengths, and appears to be fairly small for visible wavelengths as well.

4.3. Extended Laser Guide Stars

The final error source associated with wave optics phenomena is the impact of extended, three-dimensional, laser guide stars. The dotted curve in Fig. 4 plots Strehl ratio time histories including this effect. Note that performance does not begin to improve immediately because the AO loop was not closed until simulation cycle 10. This delay was included to provide the LGS pointing control loops time to converge. Performance after this point is very similar to, and actually slightly superior to, the results with ideal point source laser guide stars, indicating that the extended laser guide stars have filtered out some of the errors due to speckle noise.

The net effect of diffraction on MCAO simulation results is summarized in table 4. The values are the mean Strehls averaged over cycles 21 through 100 of the simulation. (The results presented for the geometrical model are very slightly different from table 3 above, since the results at the edge and corner of the field are for one particular field point instead of averaged over four field points.) The overall Strehl ratio losses due to diffraction correspond to RMS OPD's of about 36.3, 53.6, and 63.4 nanometers at the center, edge, and corner of the square 1 arc minute field.

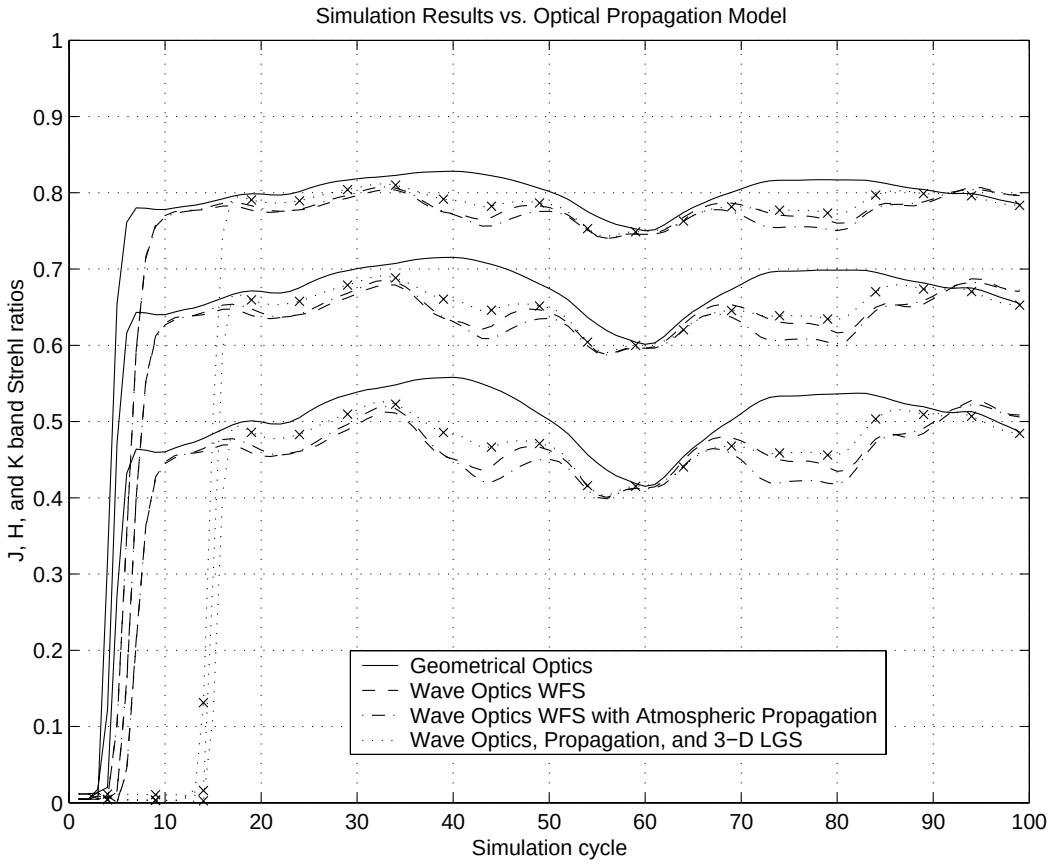

Figure 4. Impact of Optical Propagtion Model on MCAO Simulation Results

This figure is similar to Fig. 3 above, except that MCAO performance is presented for four different optical propagation models with the wavefront reconstruction algorithm held fixed. The Strehl ratios computed with extended laser guide stars do not begin to increase immediately because the AO loop was not closed until the tenth simulation cycle. This delay was included to allow the LGS pointing loops time to converge.

Spectral Band	Geometric Model			Diffraction Model		
	Center	Edge	Corner	Center	Edge	Corner
J	0.615	0.510	0.493	0.594	0.475	0.446
H	0.756	0.678	0.666	0.742	0.650	0.628
K	0.854	0.803	0.795	0.845	0.784	0.769

Table 4. Overall Impact of Diffraction Effects on MCAO Simulation Results

This table plots time-averaged Strehl ratios at the center, edge, and corner of a square 1 arc minute field of view for the atmospheric and AO system parameters summarized in Tables 1 and 2 above.

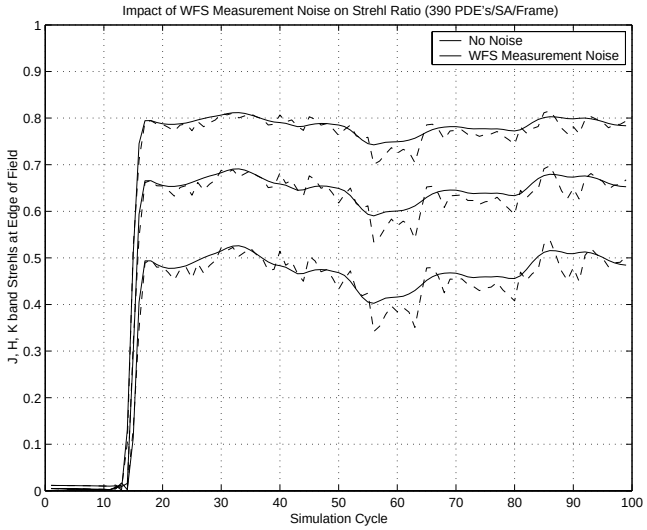

Figure 5. Impact of WFS Measurement Noise on MCAO Simulation Results

These results are similar to Fig. 4, except that they compare MCAO performance with and without LGS WFS measurement noise. Diffraction effects and three-dimensional laser guide stars are modeled, and the reconstruction algorithm has been optimized for the actual LGS WFS noise level as indicated in Table 2. The NGS WFS measurements are still noise free apart from speckle effects.

5. WFS MEASUREMENT NOISE AND DM-TO-WFS MISREGISTRATION

Figure 5 continues with the series of simulation results by including the effects of LGS WFS measurement noise. The nominal signal level is 390 photodetection events per frame for a fully illumnated subaperture, and the detector read noise is 6 electrons. The NGS WFS signal level is still infinity. The mean Strehl ratio reduction for cycles 21 through 100 of the simulation correspond to an RMS OPD of about 26.8, 33.6, and 42.3 nanometers at the center, edge, and corner of the 1 arc minute field. The overall Strehl ratio loss due to both noise and diffraction effects together corresponds to RMS OPD's of about 45.1, 63.2, and 76.2 nanometers, which is extremely close to what one would estimate by computing the RSS of the two individual effects.

The final result in this paper relates to DM misregistration and other sources of error in computing the DM-to-WFS influence matrix. These error include: (i) genuine misregistration between the DM's and the LGS WFS due to flexure and thermal effects, (ii) LGS pointing errors, and (iii) additional misregistration errors induced by the fast tip/tilt mirror, which is not located at a pupil. This last effect is estimated to be considerably smaller than the first two and has not yet been included in the simulations. The present estimate for the first error source in the Gemini MCAO system is a RMS two-axis misregistation of 0.004 times the diameter of the pupil, which we have simulated generically by placing rotation, magnification, and translation alignment errors of this magnitude on the three deformable mirrors. The pointing biases in the LGS locations on the sky are estimated to be 1 arc second (two-axis, one sigma), and these offsets introduce additional errors in the DM-to-WFS influence matrix by translating the LGS beamprints on the two deformable mirrors conjugate to nonzero altitudes. We have simulated these biases by picking a single set of normally distributed, zero mean pointing errors for the 5 LGS. Finally, the dynamic LGS pointing errors due to noise and servo lag in the LGS tip/tilt control loops are already modeled by the simulation.

Fig. 6 illustrates the results obtained with these sample misregistration errors. The reduction in the mean Strehl ratio averaged over cycles 21 to 100 of the simulation corresponds to RMS wave front errors of 25.9, 22.8, and 19.4 nm at the center, edge, and corner of the field. This is a useful result for designing the opto-mechanical bench for MCAO on Gemini South, since it indicates that the system is no more sensitive to representative misregistration errors than a conventional AO system.

ACKNOWLEDGEMENTS

This research was supported by the Gemini Observatory, which is operated by the Association of Universities for Research in Astronomy, Inc., under a cooperative agreement with the NSF on behalf of the Gemini Partnership:

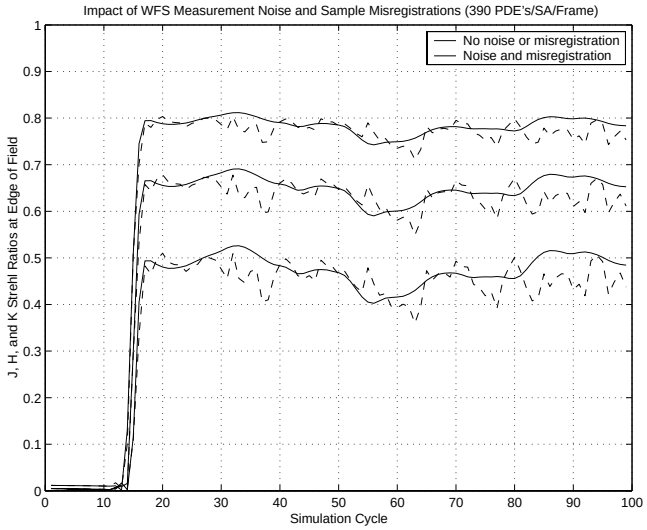

Figure 6. Impact of WFS Measurment Noise and Misregistration Errors

This figure is similar to FIg. 5, except that representative DM-to-WFS misregistration errors and LGS pointing biases have also been included in the simulation.

the National Science Foundation (United States), the Particle Physics and Astronomy Reserach Council (United Kingdom), the National Research Council (Canada), CONICYT (Chile), the Australian Reserach Council (Australia), CNPq (Brazil), and CONICET (Argentina).

REFERENCES

J.M. Beckers, "Detailed Compensation of Atmospheric Seeing using Multi-Conjugate Adaptive Optics," *SPIE* **1114**, 215–217 (1989).

B.L. Ellerbroek, "First-order performance evaluation of adaptive-optics systems for atmospheric-turbulence compensation in extended-field-of-view astronomical telescopes," *J. Opt. Soc. Am. A* **11**, 783–805 (1994).

B.L. Ellerbroek, "Scaling Multi-Conjugate Adaptive Optics Performance Estimates to Extremely Large Telescopes," *SPIE* **4007**, 1088-1099 (2000).

R. Flicker, B.L. Ellerbroek, and F.J. Rigaut, "Comparison of multiconjugate adaptive optics configurations and control algorithms for the Gemini-South 8m telescope," *SPIE* **4007**, 1032-1043 (2000).

T. Fusco, J.-M. Conan, V. Michau, L.M. Mugnier, and G. Rousset, "Phase estimation for large field of view: application to multiconjugate adaptive optics," *SPIE* **3763**, 125–133 (1999).

D.C. Johnston and B.M. Welsh, "Analysis of multiconjugate adaptive optics," *J. Opt. Soc. Am. A* **11**, 394–408 (1994).

G.A. Tyler, "Merging: a new method for tomography through random media," *J. Opt. Soc. Am. A* **11**, 409–424 (1994).

J. Vernin, A. Agabi, R. Avila, M. Azouit, R. Conan, F. Martin, E.Masciadri, L. Sanchez, and A. Ziad, *1998 Gemini Site Testing Campaign: Cerro Pachon and Cerro Tololo*, (Gemini Project, 2000).

E.P. Walner, "Optimal wave-front correction using slope measurements," *J. Opt. Soc. Am.* **73**, 1771–1776 (1983).

B.M. Welsh and C.S. Gardner, "Effects of turbulence-induced anisoplanatism on the imaging performance of adaptive-astronomical telescopes using laser guide stars," *J. Opt. Soc. Am. A* **8**, 69–80 (1991).